International Immunopharmacology 164 (2025) 115382

Contents lists available at ScienceDirect

International Immunopharmacology

journal homepage: www.elsevier.com/locate/intimp

Baicalein mitigates chlorpyrifos-induced intestinal injury by blocking AMPK–ULK1 binding via the autophagy/ferroptosis axis

Huanqi Zhang [a], Xiaozhe Chen [a], Fuqing Liu [a], Yanju Bi [b], Meichen Gao [b], Xiaojing Li [a,*]

[a] College of Animal Science and Technology, Northeast Agricultural University, Harbin 150030, PR China
[b] College of Veterinary Medicine, Northeast Agricultural University, Harbin 150030, PR China

ARTICLE INFO

Editor: Yi-Chao Zheng

Keywords:
Chlorpyrifos
Baicalein
AMPK–ULK1
Autophagy
Ferroptosis

ABSTRACT

Long-term environmental exposure to chlorpyrifos (CPF) can cause intestinal damage. Baicalein (BAI) helps aquatic organisms resist environmental pollution stress. Adenosine 5′-monophosphate activated protein kinase (AMPK) is a key molecule in energy regulation; however, the mechanism by which BAI inhibits CPF-induced autophagy/ferroptosis remains unclear. Based on reported environmental concentrations and IC_{50} values of CPF, we established models using the midgut of carp and Epithelioma papulosum cyprini (EPC) cells exposed to CPF with or without BAI treatment. Transcriptomics and network pharmacology were used to analyze the key pathways affected by CPF and BAI. Tissue damage, cell cycle regulation, autophagy, ferroptosis, and mitochondrial function were assessed. The effect of BAI on AMPK–unc-51-like autophagy-activating kinase 1 (ULK1) binding was confirmed by molecular dynamics simulation, co-immunoprecipitation, and laser confocal analysis. In addition, the regulatory impact of an AMPK activator on the autophagy/ferroptosis axis was examined. Results indicated that BAI alleviated CPF-induced pathological changes and mitochondrial damage. CPF exposure caused tight junction disruption, mitochondrial depolarization, and reactive oxygen species and mitochondrial reactive oxygen species production. Transcriptomic analysis revealed that CPF toxicity is related to phagosomes, cell cycle regulation, and ferroptosis. By targeting AMPK, BAI prevents the formation of the AMPK–ULK1 complex and inhibits the CPF-induced cascade involving excessive autophagy, cell cycle arrest, and ferroptosis. In conclusion, BAI targets AMPK to prevent binding with ULK1, thereby suppressing the CPF-activated autophagy/ferroptosis axis, reversing mitochondrial dysfunction, and restoring intestinal homeostasis.

1. Introduction

Organophosphorus pesticides, used as insecticides have emerged as alternatives to organochlorine and carbamate pesticides in many countries. Chlorpyrifos [O,O-diethyl-O-(3,5,6-trichloro-2-pyridinyl) phosphorothioate; CPF] is the fourth most widely used pesticide worldwide [1]. The World Health Organization (WHO) has classified CPF as a class II toxic pesticide, indicating it is safer than other organophosphorus pesticides, leading to its misuse and overuse in agricultural production [2]. Notably, only 0.1 % of CPF is effective against target pests, while the remaining 90 % persists in the environment, contaminating water bodies through surface runoff [3]. CPF has been detected in water sources worldwide. The residual concentrations of CPF reached up to 8 μg/L in the surface water of Lake Tana [4], approximately 70 μg/L in Philippine [5], 37.3 μg/L in Nagarpur and Saturia upazilas [6], and 23.02 μg/L in El Albujón watercourse [7]. Water and food are the primary pathways through which CPF enters the human body, and the gastrointestinal tract is the first site exposed to food contaminants [8]. Intestinal epithelial cells play an important role in food digestion and immune regulation. CPF exposure results in epithelial hyperplasia, edema, and degeneration, eventually leading to impaired intestinal function [9]. CPF causes intestinal barrier damage and alters intestinal mucosal permeability in *Rattus norvegicus*, *Mus musculus*, *Apis mellifera*, and *Apis ceran* [10–12]. Therefore, there is an urgent need to develop

Abbreviations: AMPK, Adenosine 5′-monophosphate-activated protein kinase; ATG5, Autophagy-related gene 5; ATG12, Autophagy-related gene 12; BAI, Baicalein; CPF, Chlorpyrifos; CQ, Chloroquine; EPC, Carp Epithelioma papulosum cyprinid; Fer-1, Ferrostatin-1; FTH, ferritin heavy chain; GPX4, Glutathione peroxidase 4; LC3, light chain 3; mtROS, mitochondrial ROS; NCOA4, Nuclear receptor coactivator 4; ROS, Reactive oxygen species; ULK1, Unc-51-like autophagy-activated kinase 1.

* Corresponding author.
E-mail address: xiaojingli@neau.edu.cn (X. Li).

https://doi.org/10.1016/j.intimp.2025.115382
Received 29 May 2025; Received in revised form 30 July 2025; Accepted 13 August 2025
Available online 19 August 2025

safe and effective drugs to treat the effects of CPF contamination.

Ferroptosis, a recently discovered form of cell death related to cellular iron homeostasis, may represent a promising therapeutic target for maintaining intestinal health [13]. The intestinal epithelium can regulate the concentration of iron ions in the body [14], and ferroptosis is activated when iron metabolism is disrupted or when glutathione peroxidase 4 (GPX4) is inactivated [15]. Previous studies have demonstrated that inhibiting ferroptosis can alleviate CPF-induced hepatotoxicity in a zebrafish model, suggesting a potential intervention approach [16]. Excessive iron accumulation activates ferroptosis through reactive oxygen species (ROS) generated by the Fenton reaction in mitochondria [17]. Autophagy may promote cell survival; however, excessive autophagy combined with impaired lysosomal activity is an important driver of ferroptosis. The fusion of lysosomes and autophagosomes provides degradation capacity. When lysosomal activity is compromised, autophagic flux increases, resulting in excessive autophagy [18]. High expression of ATG family proteins promotes iron accumulation and triggers ferroptosis [19]. Wu et al. demonstrated that CPF exposure increased autophagy through the protein kinase B (AKT) pathway, leading to kidney damage in carp [20]. Adenosine 5′-monophosphate activated protein kinase (AMPK) signaling is involved in various cellular processes, including lipid metabolism and mitochondrial homeostasis [21]. AMPK phosphorylates unc-51-like autophagy-activated kinase 1 (ULK1) and inhibits mammalian target of rapamycin (mTOR)-driven autophagy activation [22]. Studies have demonstrated that exposure to multiple toxicants, such as pesticides, heavy metals, plasticizers and chemical contaminants, activates the AMPK pathway [23–25].

Baicalein (BAI) is a flavonoid monomer isolated from *Scutellaria baicalensis* Georgi, which has anti-inflammatory, anticancer, and antioxidant properties [26], and can resist tissue damage caused by the environmental pollutant cadmium [27]. Remarkably, BAI and its metabolites are abundant in the intestine after oral administration, providing effective protection of the intestine [28]. BAI is increasingly recognized as a natural ferroptosis inhibitor. A animal model study has reported that BAI inhibits ferroptosis to alleviate cisplatin-induced renal injury [29]. In addition, BAI has been reported to reduce ferroptosis after lipid peroxidation in HK2 cells [30]. However, the mechanism underlying the protective effect of BAI against ferroptosis in the intestine remains unclear. The origin and structure of the human body is highly similar to that of fish. The use fish instead of mice and rats as model organisms is increasingly being favored [31]. In this study, we established carp midgut and Epithelioma papulosum cyprini (EPC) cells model of CPF poisoning and/or BAI intervention and observed the following: (1) BAI reduces CPF-induced intestinal toxicity and inhibits epithelial cell death in carp; (2) transcriptomic studies revealed that CPF toxicity is associated with ferroptosis, autophagy, cell cycle regulation, and mitochondrial dysfunction; (3) BAI targets AMPK and blocks its interaction with ULK1; (4) BAI attenuates CPF-activated autophagy, ferroptosis, and cell cycle arrest, thereby restoring mitochondrial function via the AMPK–ULK1 pathway. This study provides new evidence and experimental basis for the potential of BAI as a therapeutic agent against environmental pollution-induced toxicity.

2. Materials and methods

2.1. Geographic distribution maps

ArcMap 10.8 was used to generate the geographical distribution map of pesticide use. Details are described in Supplementary 1.1.

2.2. Animals

The chemical compound CPF (CAS No. 2921-88-2; purity ≥98 %) was obtained from Shanghai Aladdin Biochemical Technology Co., Ltd. (China). BAI (CAS No. 491–67-8; purity ≥99 %) was obtained from Shanghai Macklin Biochemical Technology Co., Ltd. (China). All animal experiments were conducted according to the ethical guidelines and approved by the Ethics Committee of the Northeast Agricultural University (Approval No. NEAUEC20230250). The modeling process is illustrated in Fig. 1A. The CPF concentration used in this study was based on the LC_{50} and the reference environmental concentration (specifically, 1/25 of the 96-h LC_{50}), while the BAI dose was determined based on our previous study [20,32]. Detailed treatment protocols and dose information are provided in Supplementary 1.2. Fish were maintained in barrels containing 40 L of water. During the experimental period, they were fed twice a day (at 8:30 and 16:30). The water in the barrels was completely replaced every 2 days. Dissolved oxygen levels were maintained above 7 mg/L through continuous aeration. No mortality was observed throughout the 30-day feeding period.

2.3. Carp midgut histological observation

The carp midgut was sectioned at 3-mm thickness for hematoxylin and eosin (H&E) staining and examined under a light microscope [33]. Ultrathin sections (1 μm) were prepared, stained with uranyl acetate and lead citrate, and observed under a transmission electron microscope. Detailed procedures are described in Supplementary 1.3.

2.4. Transcriptomics

Total RNA from the carp midgut was extracted using the TRIzol method. RNA samples with high concentration and purity were sent to Bioacme Biotechnology Company (Wuhan, China) for cDNA library construction and sequencing. Differential expression analysis was conducted using the Metabo-Analyst platform (https://new.metaboanalyst.ca/) and the CNSknowall platform (https://cnsknowall.com/#/HomePage) for data visualization and interpretation.

2.5. Cell culture

The carp EPC cell line was purchased from the Wuhan University Cell Bank. Detailed culture conditions and grouping information are described in Supplementary 1.4.

2.6. Detection of mitochondrial membrane potential (MMP)

The JC-1 kit (Beyotime Biotechnology, China) was used to determine MMP in EPC cells from each group, following the manufacturer's instructions. The fluorescence of JC-1 monomers and J-aggregates was observed at excitation wavelengths of 530 and 590 nm, respectively, using a fluorescence microscope (Thermo Fisher Scientific, USA) and a flow cytometer (NovoCyte, Agilent Technologies).

2.7. Cell cycle detection

Cell cycle was analyzed using a kit (Solarbio, CA1510) according to manufacturer's instructions and detected using flow cytometry (NovoCyte, Agilent Technologies).

2.8. Detection of ROS and mtROS

DCFH-DA fluorescent probe (Nanjing Jianchang Bioengineering Institute, China) was used to measure intracellular ROS production, while MitoSOX Red probe (ABclonal Technology, China) was used to evaluate mtROS levels. Fluorescence signals were observed using fluorescence microscopy.

2.9. Determination of iron content and assessment of antioxidant capacity

The antioxidant capacity indicators, including Total Antioxidant

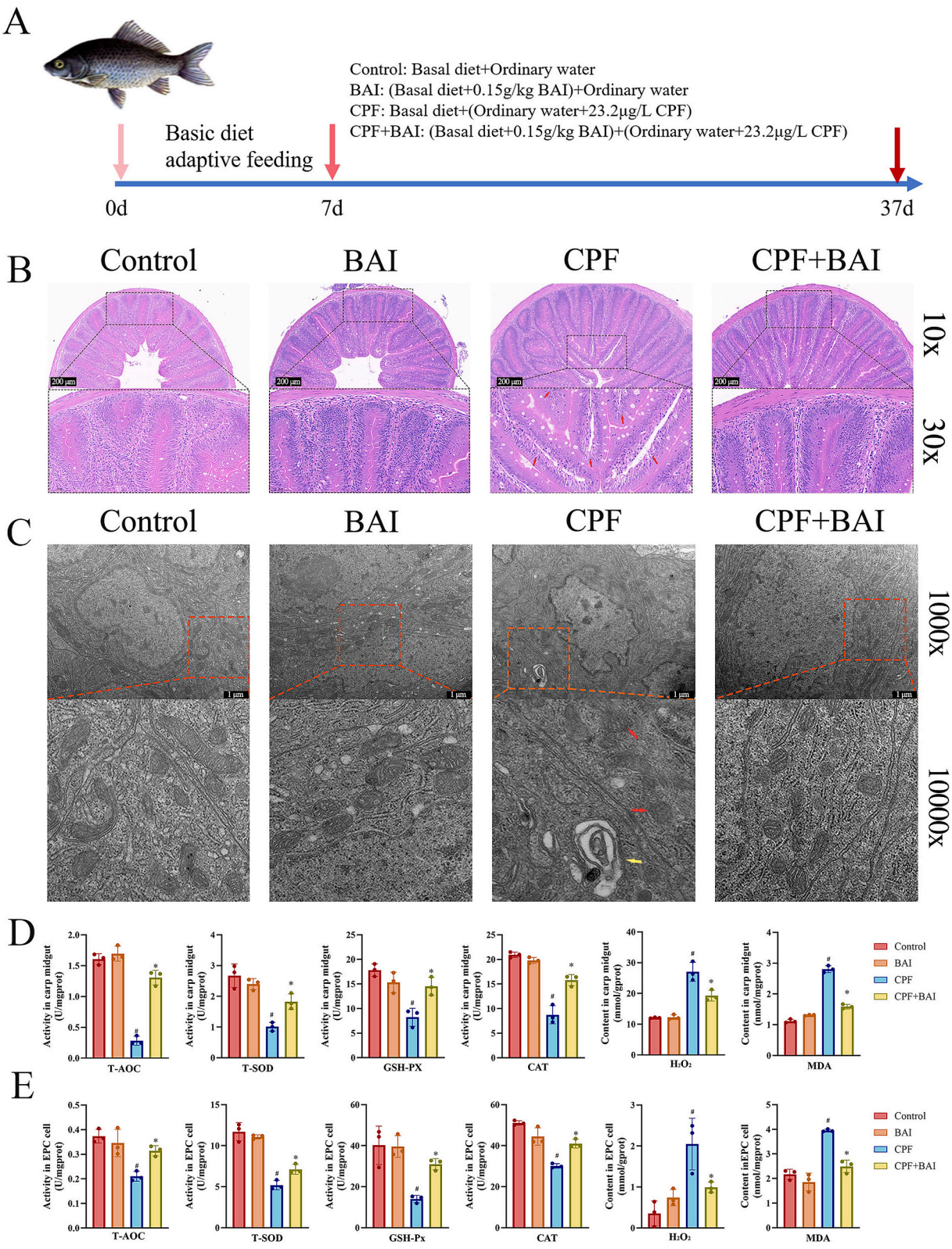

Fig. 1. BAI counteracts carp midgut and EPC cells damage induced by CPF. (**A**) Schematic diagram of animal model establishment. (**B**) H&E staining of carp midgut. (**C**) Transmission electron microscopy (TEM) was used to observe the micromorphological changes of carp midgut. (**D-E**) Oxidative stress and antioxidant capacity evaluation in carp midgut and EPC cells. $^{\#}$Represents the statistical difference between the group and the Control group. *Represents the statistical difference between the group and the CPF group. All data were shown as mean ± SD ($n = 3$). $^{*}P < 0.05$, $^{\#}P < 0.05$.

Capacity (T-AOC), Total Superoxide Dismutase (T-SOD), Malondialdehyde (MDA), Glutathione Peroxidase (GSH-Px), CATalase (CAT), Hydrogen Peroxide (H_2O_2), and iron content were measured using kits from the Nanjing Jianchang Bioengineering Institute (China).

2.10. Target screening

Network pharmacology was used to analyze the action pathway of BAI. Molecular dynamics (MD) simulations, cellular thermal shift assay (CETSA) and drug affinity responsive target stability (DARTS) assays were used to determine BAI binding targets. Detailed methods are described in Supplementary 1.4.

2.11. Molecular docking

The structures of the AMPK and ULK1 protein were screened using the Uniprot database (https://www.uniprot.org/). The 3D structure of BAI was downloaded from the PubChem database (https://pubchem.ncbi.nlm.nih.gov/). Molecular docking simulations were performed using AutoDock 1.5.7, and the resulting 3D complexes were visualized using PyMoL 2.6.0.

2.12. Co-immunoprecipitation assay

Protein–protein binding was assessed using co-immunoprecipitation and western blotting (Absin, abs955). Briefly, 4 μg of AMPK antibody (Abmart) or IgG control antibody (ABclonal) were added to cell lysates and incubated overnight at 4 °C. Subsequently, 5 μL each of protein A and protein G beads were added and incubated overnight at 4 °C. This mixture was centrifuged at 12000 ×*g* for 1 min, washed five times with 1 × Wash Buffer, and precipitates were resuspended in 40 μL SDS buffer, subsequently heated at 95 °C for 5 min.

2.13. Immunofluorescence

Cells were blocked with TBSTx containing 5 % bovine serum albumin (BSA, Yeasen) for 60 min. Primary antibodies against AMPK (1100, Abmart), ULK1 (1100, Abmart), GPX4 (1:100, ABclonal), FTH (1:100, ABclonal), LC3 (1100, ABclonal) and p62/SQSTM1 (1100, ABclonal) were incubated overnight at 4 °C. Secondary antibodies, DyLight 594 goat anti-rabbit IgG and Alexa Fluor 488 goat anti-rabbit IgG (1, 1000, Biodragon Immunotechnology, China), were applied for 2 h at 25 °C temperature. After washing with TBSTx for 15 min, nuclei were stained with DAPI (Beyotime, China) for 5 min.

2.14. Real-time quantitative PCR (qRT-PCR)

Total RNA was extracted from each group using TRIzol reagent. Quantitative PCR was performed using SYBR Green dye (AQ132–11, TransGen) on a LightCycler® 96 System (Roche). Primer sequences are listed in Table S1. mRNA expression levels were calculated using the $2^{-\Delta\Delta Ct}$ method, with β-actin and 18S rRNA serving as internal controls.

2.15. Western blot

Proteins were separated by 10 % SDS-PAGE, and transferred to a nitrocellulose membrane using a Tris-glycine buffer system. Membranes were blocked with Minute Block (AIWB-004, Affinibody LifeScience Co. Ltd., China) at 37 °C for 10 min and incubated overnight with the primary antibodies as listed in Table S2. Membrane were subsequently incubated with the secondary antibody (anti-rabbit IgG, 1:10,000, Immunoway, China) for 60 min. Protein bands were visualized using a chemiluminescence system (Applygen Technologies, China). Quantitative analysis of band intensity was performed using ImageJ software, with β-actin as the loading for normalization.

2.16. Statistical analysis

All data are presented as mean ± standard deviation (SD). Statistical analyses were performed using GraphPad Prism 9.5. Differences between groups were analyzed by one-way ANOVA followed by Tukey's post-hoc multiple comparison test using GraphPad Prism 8. * and # indicate statistically significant difference ($P < 0.05$) compared with the CPF and control groups, respectively.

3. Results

3.1. Pesticides and CPF co-occur geographically worldwide

Preliminary data screening yielded global pesticide use (Fig. S1A) and CPF residue reports (Fig. S1B). These were found to be distributed across common geographical regions. Brazil, the United States of America, Indonesia, China, and Argentina ranked as the top five countries in pesticide use. The top three countries reporting CPF residues were China, India, and the United States of America. Concurrently, Asia ranked second and first in pesticide use (Table S3) and residue reporting (Table S4), respectively. These findings indicate that pesticide use and CPF residues are prevalent in overlapping regions worldwide.

3.2. BAI feeding attenuated CPF-induced midgut damage in carp

Based on the environmental residual concentration of CPF [6] and its IC_{50} value [34], a CPF concentration of 23.2 μg/L in water was selected to establish a CPF poisoning model in carp. The effect of BAI was determined by feeding carp with 0.15 g/kg BAI (Fig. 1A). H&E staining results revealed histopathological changes in the carp midgut (Fig. 1B). The CPF group exhibited intestinal villus rupture, disorganized interstitial cells, vacuolar degeneration of lower cells, and infiltration of inflammatory cells (red arrows). Addition of BAI markedly improved midgut structure compared to the CPF-only group. In the CPF group, autophagic vacuoles (yellow arrow) and characteristic mitochondrial damage (red arrows), including blurred double-layer membranes and ridge breakage, were observed. However, BAI treatment restored mitochondrial morphology (Fig. 1C). The CCK8 assay was used to select in vitro doses of 25 μM CPF and 30 μM BAI for subsequent experiments (Fig. S2A and B). Using these doses, we assessed the redox balance–related indicators. Compared with the control group, CPF significantly inhibited the activities of T-AOC, T-SOD, GSH-Px, and CAT ($P < 0.05$) and significantly increased oxidative stress markers H_2O_2 and MDA ($P < 0.05$). BAI reduced intestinal oxidative stress, restored antioxidant enzyme activities, and reactivated the antioxidant system (Fig. 1D). These findings were consistent with antioxidant capacity results obtained from carp intestinal tissue in vivo (Fig. 1E). In addition, CPF disrupted the tight junction network, whereas BAI supplementation alleviated this damage (Fig. S2C and D).

3.3. Effect of CPF exposure on carp midgut transcriptomics

To clarify the effect of CPF on the carp midgut, RNA-seq analysis was performed on midgut tissue samples. Initially, raw data were normalized (Fig. 2A). Principal component analysis (PCA) plots (Fig. 2B and C) clearly illustrated the distinct transcriptional differences between the control and CPF-exposed groups. Annotated differentially expressed genes (DEGs) were utilized to generate a volcano plot, revealing 170 significantly downregulated and 441 significantly upregulated genes. (Fig. 2D). The top 100 DEGs were selected according to the *P* value and displayed on the heatmap to show the DEGs in the midgut of carp exposed to CPF (Fig. 2E).

Further analysis via KEGG revealed differential enrichment in pathways such as phagosome, cell cycle, ferroptosis, fatty acid biosynthesis, DNA replication, and various metabolic pathways (Fig. 2F). A radar plot showed that CPF exposure was closely related to iron ion

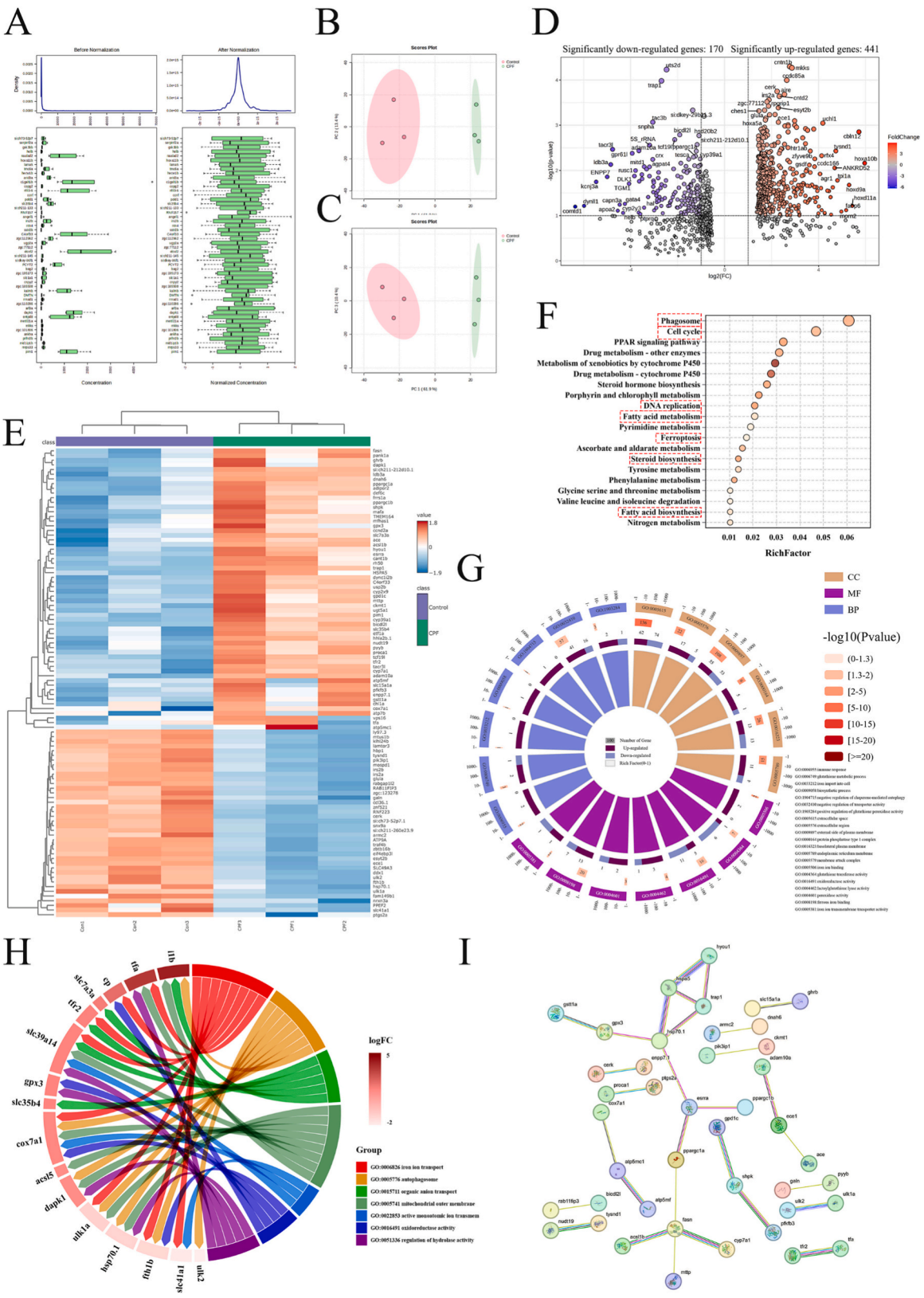

Fig. 2. Transcriptome results of the carp midgut exposed to CPF. (**A**) Normalized processing of transcriptome sequencing raw data. (**B**—**C**) Principal component analysis (PCA) revealed the overall gene expression pattern in the intestines of carp after exposure. (**D**) The differential volcano plot shows the upregulation and downregulation distribution of DEGs caused by CPF exposure. (**E**) Hierarchical clustering heatmaps of 3 groups of Control and 3 groups of CPF treatment. (**F**) KEGG enrichment analysis results in CON vs CPF. (**G**) GO enrichment pathway results of CON vs CPF. (**H**) GO analysis results of DEGs in CON vs CPF. (**I**) Protein-protein interaction network of DEGs. All data were shown as mean ± SD (n = 3).

transport, transmembrane transport, oxidation-reduction reactions, glutathione metabolism, and cell membrane function (Fig. 2G). DEGs involved in most of the pathways shown in Fig. 2G were selected for gene ontology (GO) enrichment analysis. The GO network plot exhibited significant enrichment in autophagosomes and the mitochondrial outer membrane following CPF exposure (Fig. 2H). In addition, the protein-protein interaction (PPI) network revealed key interactions among AMPK pathway (atp5mc1, atp5mf, ppargc1b, and ppargc1a), lipid metabolism (fasn, cyp7a1, and mttp), other metabolic pathways (esrra, gstt1a, cerk, mnudt19, shpk, and pfkfb3), and ferroptosis (ptgs2a, cox7a1, gpx3, and acsl1b) (Fig. 2I). Collectively, these results suggest that CPF-induced intestinal damage in carp may involve autophagy, cell cycle, ferroptosis, and altered metabolic pathways.

3.4. BAI alleviated CPF-induced ferroptosis in carp midgut

Transcriptomic gene set enrichment analysis (GSEA) revealed that the processes related to iron ion transport and glutathione metabolism were highly enriched in the CPF-treated group (Fig. 3A). Ferroptosis-related features were observed using transmission electron microscopy (Fig. 1C), and the expression of ferroptosis-related genes was assessed in both the control and CPF-exposed groups (Fig. 3B). Excess iron accumulation is a major trigger of ferroptosis. Compared with the control, iron content in the intestinal tissue and EPC cells of CPF-treated carp was approximately 1.5 times higher. (Fig. 3C and D). BAI effectively reversed the iron overload ($p < 0.05$). The ferroptosis marker gene *GPX4*, the iron utilization genes *FTH* and *FTL*, and the iron efflux gene *FPN* were downregulated ($p < 0.05$). Abnormal expression of iron transport genes *TF*, *TFR1* and *TFR2* (Fig. 3E-H) was additionally noted. BAI significantly improved the abnormal expression of the abovementioned genes and restored intestinal iron transport function ($p < 0.05$). BAI reversed the CPF-induced decrease in the colocalization of GPX4 and FTH, as observed via immunofluorescence, providing further evidence of the effects of BAI on the expression of these genes (Fig. 3I and J). In addition, the ferroptosis inhibitor ferrostatin-1 (Fer-1) and the autophagy inhibitor cloroquine (CQ) effectively alleviated CPF-induced ferroptosis (Fig. S3A-E).

3.5. BAI antagonized CPF-induced autophagy in carp intestine and EPC cells

Autophagy-related pathways were enriched in RNA-seq GSEA (Fig. 4A). Differential expression of autophagy-related genes between CON and CPF groups was identified based on RNA-seq data (Fig. 4B). We found that CPF exposure increased the protein and mRNA expression levels of LC3B, Beclin1, ATG5, and ATG12 ($P < 0.05$), and decreased the expression levels of p62 ($P < 0.05$) in both carp intestine and EPC cells. Compared with the CPF group, BAI intervention increased p62 expression ($P < 0.05$) and decreased the expression of LC3, Beclin1, ATG5, and ATG12 ($P < 0.05$) (Fig. 4C-F). CPF exposure significantly increased the fluorescence intensity of LC3B and significantly decreased the fluorescence intensity of p62 in EPC cells (Fig. 4G and H). BAI effectively alleviated the abnormal changes in LC3B and p62 expression ($P < 0.05$). Lysosomes, which serve as the core degradation organelles in autophagy, were reduced in number following CPF exposure; this reduction was ameliorated by BAI (Fig. 4I and J). In addition, treatment with Fer-1 or CQ increased p62 fluorescence intensity and decreased LC3B fluorescence intensity and lysosomal damage induced by CPF (Fig. S4A—C). Both inhibitors normalized the aberrant mRNA and protein expression of autophagy-related markers, indicating that autophagic flux was blocked (Fig. S4D and E). These data indicate that BAI-mediated inhibition of CPF-induced autophagy and ferroptosis are mutually reinforcing.

3.6. BAI improved cell cycle arrest induced by CPF exposure

KEGG analysis (Fig. 2F) and GSEA (Fig. 5A) revealed that CPF toxicity was associated with the cell cycle. Most cyclin genes identified by RNA-seq were upregulated after CPF exposure (Fig. 5B). Flow cytometry analysis confirmed that CPF induced the progression from G1 to S phase (Fig. 5C). In addition, BAI treatment effectively enhanced the transcript levels of p53 and p21 in CPF-exposed carp midgut and EPC cells, while reducing the mRNA expression of Cyclin A1, Cyclin B, and Cyclin (Fig. 5D). These results suggest that BAI can attenuate CPF-induced cell cycle arrest.

3.7. Mitochondria are involved in the antagonistic effect of BAI on CPF toxicity

We screened the transcriptome for mitochondria-related genes. The results indicated that CPF exposure altered the expression of mitochondrial solute carrier (SLC) family genes, resulting in mitochondrial metabolic disorders (Fig. 6A). GSEA revealed that mitochondrial-related components were enriched in the CPF group (Fig. 6B). Fluorescence quantification (Fig. 6C and D) and flow cytometry analysis (Fig. 6E and F) demonstrated that BAI reversed CPF-induced mitochondrial depolarization. BAI scavenged intracellular ROS (Fig. 6 G and H) and mtROS (Fig. 6 I and J) levels after CPF exposure, thereby alleviating oxidative mitochondrial damage. In addition, treatment with Fer-1 or CQ restored MMP and reduced CPF-induced mtROS levels in EPC cells (Fig. S5A—F). These results confirmed that autophagy and ferroptosis act as upstream pathways of mitochondrial damage, and that BAI mitigates mitochondrial dysfunction by inhibiting CPF-induced autophagy and ferroptosis in EPC cells.

3.8. Network pharmacology analysis of BAI targets

A total of 240 BAI-associated targets were identified from the Pubchem and CTD databases (Fig. 7A). The most enriched pathways associated with CPF toxicity in RNA-seq were autophagy and cell cycle regulation (Fig. 2F). We crossed the BAI target genes, autophagy- and cell cycle related–genes to obtain 125 overlapping genes (Fig. 7B). After screening, we identified 36 key genes implicated in the modulation of autophagy and cell cycle processes by BAI (Fig. 7C). GO enrichment analysis indicated that these genes were primarily associated with the protein kinase complex and nucleotide-activated protein kinase complex (Fig. 7D). AMPK, which can regulate metabolism, was identified as a key molecule from the GO enrichment results. In the KEGG pathway, 36 key genes were enriched. The AMPK pathway, the regulation of lipolysis in adipocytes, cell cycle, and the ferroptosis pathway were in the top 20. The AMPK signaling pathway was enriched in 10 genes of this pathway (Fig. 7E).

3.9. BAI inhibited AMPK–ULK1 binding by targeting AMPK

AMPK has the potential to regulate autophagy and the cell cycle [35]. In the MD simulations, the root mean square deviation (RMSD) values of the BAI-AMPK complex fluctuated within a narrow range, indicating structural stability during the 60 ns simulation. Root mean square fluctuation (RMSF) analysis confirmed that BAI stabilized the AMPK region comprising residues 1915–1929, indicating a flexible yet stable interaction. In addition, the number of hydrogen bonds generated by the BAI–AMPK complex remained consistently between 160 and 200 throughout the simulation (Fig. 8A). To verify BAI–AMPK binding, we conducted CETSA and DARTS experiments. The CETSA assay revealed that BAI notably enhanced the thermal stability of AMPK, as indicated by a slower decline in AMPK expression in BAI-treated cells than in DMSO-treated cells (Fig. 8B). Additionally, DARTS results indicated that protease-induced AMPK degradation was significantly inhibited following BAI treatment (Fig. 8C). Molecular docking was used to

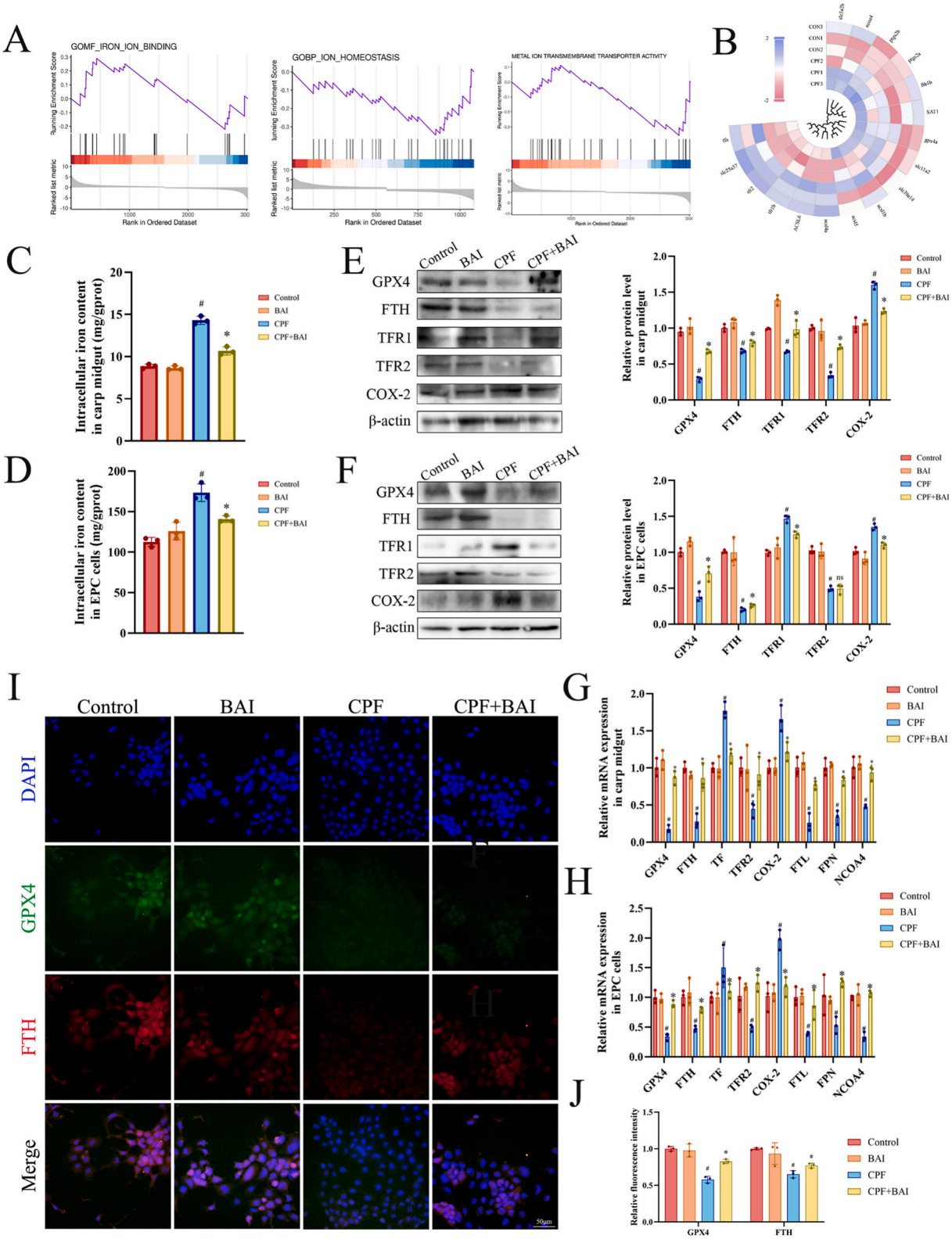

Fig. 3. BAI alleviates CPF-induced ferroptosis in carp intestine and EPC cells. (**A**) GSEA enrichment results of carp midgut transcriptomics. (**B**) Expression distribution of ferroptosis-related genes in 3 groups of Control and 3 groups of CPF treatment. (**C—D**) Iron content in carp intestine and EPC cells. (***E*-F**) Detection results of ferroptosis-related protein. (**G-H**) The ferroptosis related mRNA levels. (**I-J**) Immunofluorescence detection of ferroptosis marker protein GPX4 and FTH expression. $^{\#}$Represents the statistical difference between the group and the Control group. *Represents the statistical difference between the group and the CPF group. Ns represents the no statistical difference between the group and the CPF group. All data were shown as mean ± SD (n = 3). *P < 0.05, $^{\#}$P < 0.05.

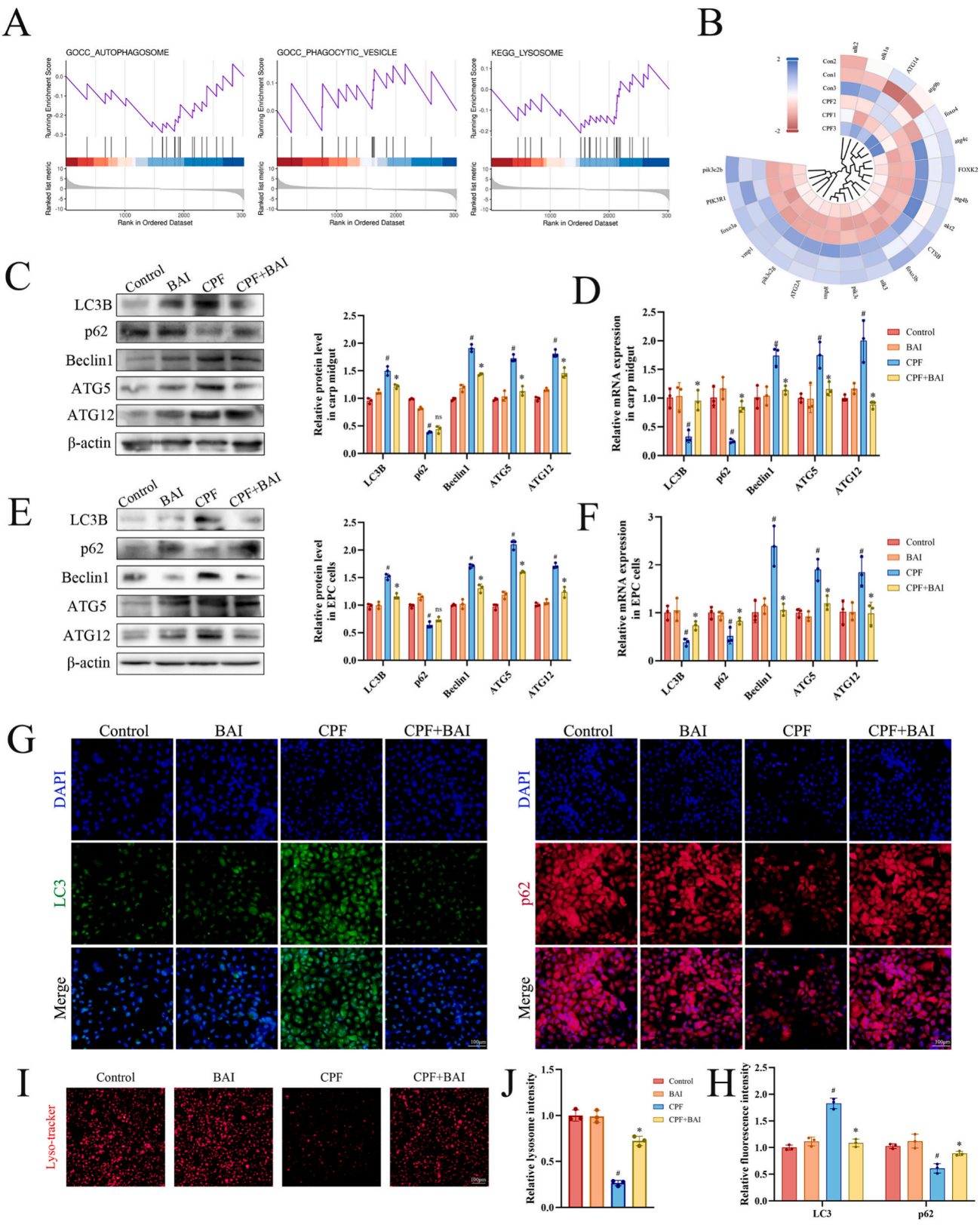

Fig. 4. Effect of CPF exposure/BAI interaction on autophagy. (**A**) GSEA enrichment results of carp midgut transcriptomics. (**B**) Circular heatmaps of autophagy-related gene expression in transcriptomics. (**C—D**) The protein and mRNA expressions of autophagy-related genes in the carp intestine. (**E-F**) Autophagy marker protein and mRNA expression levels in EPC cells. (**G-H**) Immunofluorescence detection of LC3 and p62 expression in EPC cells. (**I-J**) Lyso-tracker (50 nM) stained lysosome of EPC cells. $^{\#}$Represents the statistical difference between the group and the Control group. *Represents the statistical difference between the group and the CPF group. Ns represents the no statistical difference between the group and the CPF group. All data were shown as mean ± SD (n = 3). *P < 0.05, $^{\#}$P < 0.05.

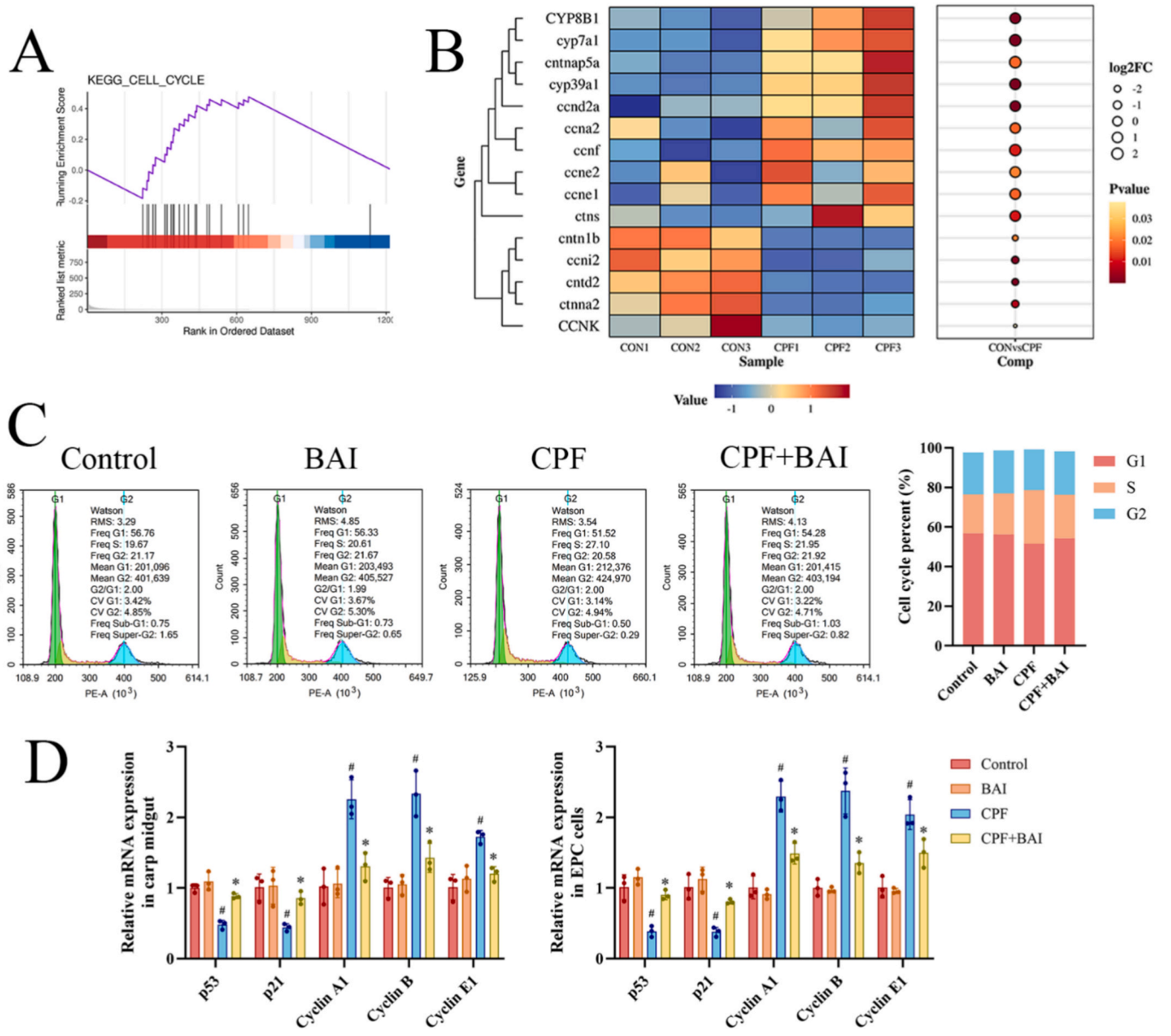

Fig. 5. Cell cycle analysis. (**A**) GSEA enrichment. (**B**) Transcriptome heat map of carp. (**C**) Cell cycle detection and visualization by flow cytometry in EPC cells. (**D**) Determination of mRNA transcription levels in carp midgut and EPC cells. #Represents the statistical difference between the group and the Control group. *Represents the statistical difference between the group and the CPF group. All data were shown as mean ± SD (n = 3). *P < 0.05, #P < 0.05.

further investigate the mechanism by which BAI regulates the AMPK pathway. The results indicated that BAI binds to Arginine (Arg) 107 and Glutamine (Gln) 109 residues of the AMPK receptor protein via hydrogen bonding (Fig. 8D). Collectively, our results support AMPK as a potential novel therapeutic target for BAI. Surprisingly, Arg107 and Gln109 are the binding sites of AMPK–ULK1, suggesting that BAI occupies the protein-binding pocket shared by AMPK and ULK1 (Fig. 8E). Co-IP assay demonstrated physical binding between AMPK and ULK1, which was inhibited by BAI treatment in EPC cells (Fig. 8F). Immunofluorescence demonstrated that the spatial co-localization of AMPK and ULK1 was reduced after BAI treatment (Fig. 8G). These results demonstrated that BAI disrupts AMPK–ULK1 binding by targeting AMPK.

3.10. BAI modified autophagy, ferroptosis and cell cycle via the AMPK pathway

To further explore the regulatory effect of BAI on AMPK, we monitored cell cycle, autophagy, and ferroptosis after treatment with an AMPK activator. BAI effectively alleviated the CPF-induced increase in both protein and mRNA expression of AMPK, ULK1, and ATG13. BAI restored mTOR mRNA expression, which was suppressed by CPF exposure, in carp intestine and EPC cells. BAI treatment alone additionally increased AMPK expression, although this change was not statistically significant compared to the control group (Fig. 9A and B). In addition, BAI inhibited the G1 to S phase transition of the cell cycle that was induced by the AMPK activator 5-Aminoimidazole-4-carboxamide ribonucleotide (AICAR) (Fig. 9C). After AICAR treatment, BAI upregulated the mRNA levels of p53 and p21 and downregulated the mRNA levels of Cyclin A1, Cyclin B, and Cyclin E1 (Fig. 9D). The autophagy marker LC3 protein was elevated and p62 protein level was decreased after AICAR treatment. BAI decreased the fluorescence intensity of LC3 and increased the fluorescence intensity of p62. Likewise, BAI enhanced the protein level of GPX4 and FTH after AICAR treatment, and promoted the spatial localization of both these proteins (Fig. 9E-G). In summary, BAI improves cell cycle arrest and reduces autophagy flux and ferroptosis by blocking the AMPK pathway.

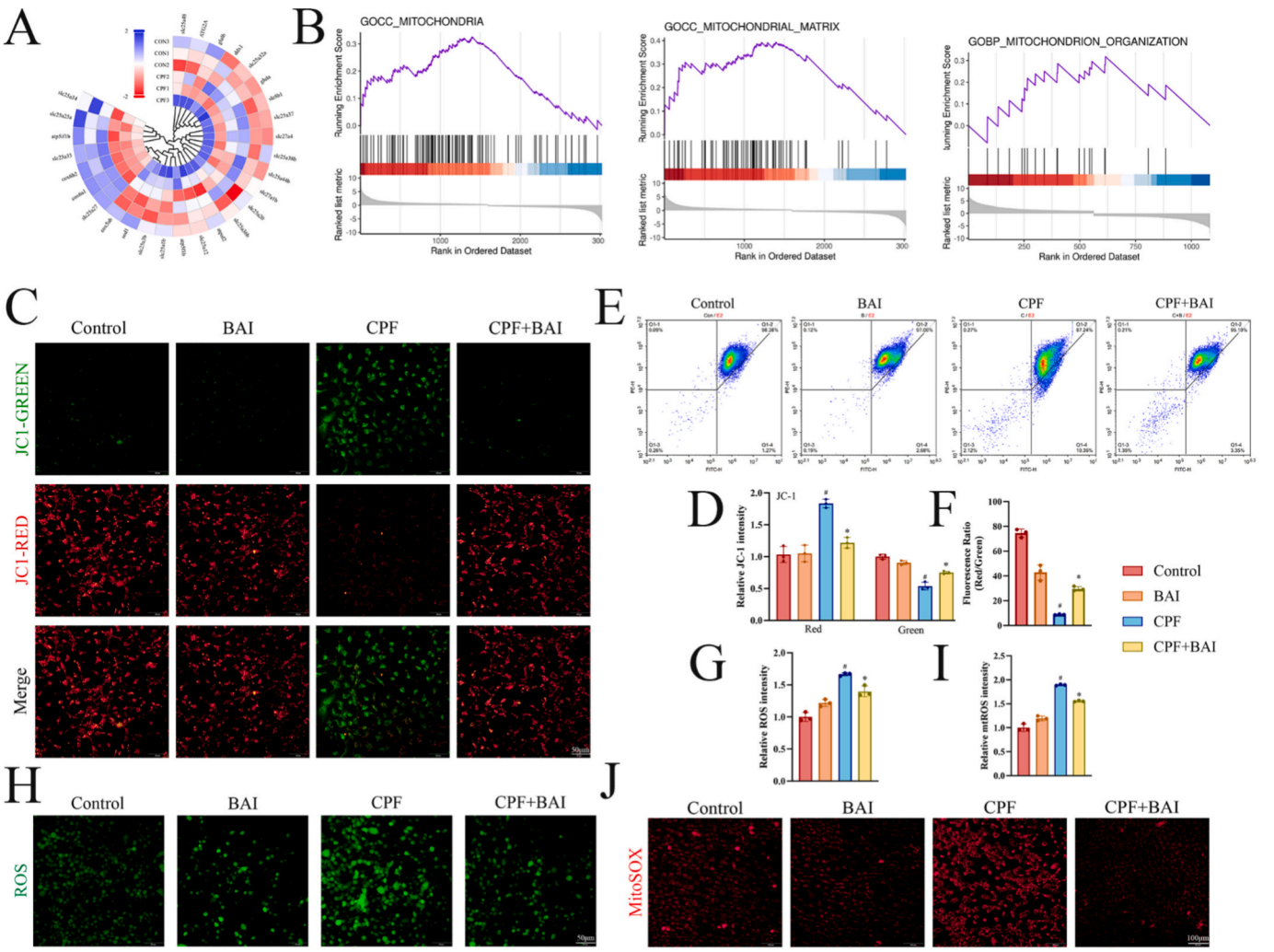

Fig. 6. Mitochondrial function assessment. (**A**) Circular heatmap of mitochondrial metabolism-related gene expression in transcriptomics. (**B**) GSEA enrichment of RNA-seq analysis in carp midgut. (**C—D**) The changes of MMP in EPC cells were detected by fluorescence quantitative method. (**E-F**) Flow cytometry was used to detect the changes of MMP in EPC cells. (**G-H**) DCFH-DA green probe was used to quantify ROS in EPC cells. (**I-J**) Quantification of mitochondrial ROS in EPC cells was performed using MitoSOX Red probes. $^{\#}$Represents the statistical difference between the group and the Control group. *Represents the statistical difference between the group and the CPF group. All data were shown as mean ± SD (n = 3). *P < 0.05, $^{\#}$P < 0.05. (For interpretation of the references to colour in this figure legend, the reader is referred to the web version of this article.)

4. Discussion

CPF is considered a potential environmental risk due to its widespread presence in various water sources. CPF residues have contributed to global water pollution and harmed the sustainable development of fish populations [36]. Exposure to CPF causes epithelial hyperplasia, edema, and degeneration, ultimately leading to impaired intestinal function [9]. It has been confirmed that autophagy is involved in the early stages of ferroptosis, and that AMPK activation induces autophagy-dependent ferroptosis [37]. Moreover, autophagy and ferroptosis are closely linked to the regulation of the cell cycle [38,39]. In this study, we found that CPF caused intestinal villus rupture, autophagic vacuole formation, mitochondrial double-layer membrane blurring, and ridge breakage. RNA-seq analysis revealed that CPF-induced intestinal damage involved pathways related to phagosome formation, cell cycle regulation, ferroptosis, fatty acid biosynthesis, DNA replication, and various metabolic processes. BAI addition alleviated CPF-induced tissue damage and modulated autophagy, cell cycle arrest, and ferroptosis. Network pharmacology analysis demonstrated that the regulation of autophagy and cell cycle by BAI was closely linked to the AMPK pathway. Further experiments confirmed that BAI targets AMPK, preventing its binding with ULK1. In addition, BAI inhibits the AMPK pathway mediated by AMPK activators to ameliorate cell cycle disorders and improve the regulation of autophagy, and ferroptosis, thereby reducing cell damage.

AMPK is a sensor that regulates lipid homeostasis, mitochondrial homeostasis and metabolic pathways to determine cell fate [21,40]. Under glucose starvation, AMPK phosphorylates ULK1 at serine (Ser) 317 and Ser777 to activate ULK1 kinase [41]. AMPK phosphorylates the Ser556 site to enhance ULK1 activity and increase autophagy [42]. Herzig et al. believed that there are at least four direct interaction sites between AMPK and ULK1: Ser467, Ser555, threonine (Thr) 574, and Ser637 [21]. Bach et al. further reported that Thr180 is an important site for AMPK to phosphorylate ULK1 [43]. Therefore, other direct binding sites between AMPK and ULK1 may remain undiscovered. Our modeling analysis found that BAI occupies Arg107 and Gln109 binding sites on AMPK and ULK1simultaneously. MD simulation and CETSA and DARTS analysis confirmed that BAI targets AMPK. Mack et al. confirmed that AMPK interacts with the ULK1 spacer region and that this interaction is independent on the N-terminal region, C-domain, and kinase activity [44]. Unexpectedly, the experiment discovered that BAI blocks AMPK–ULK1 binding by targeting the Arg107 and Gln109 sites located

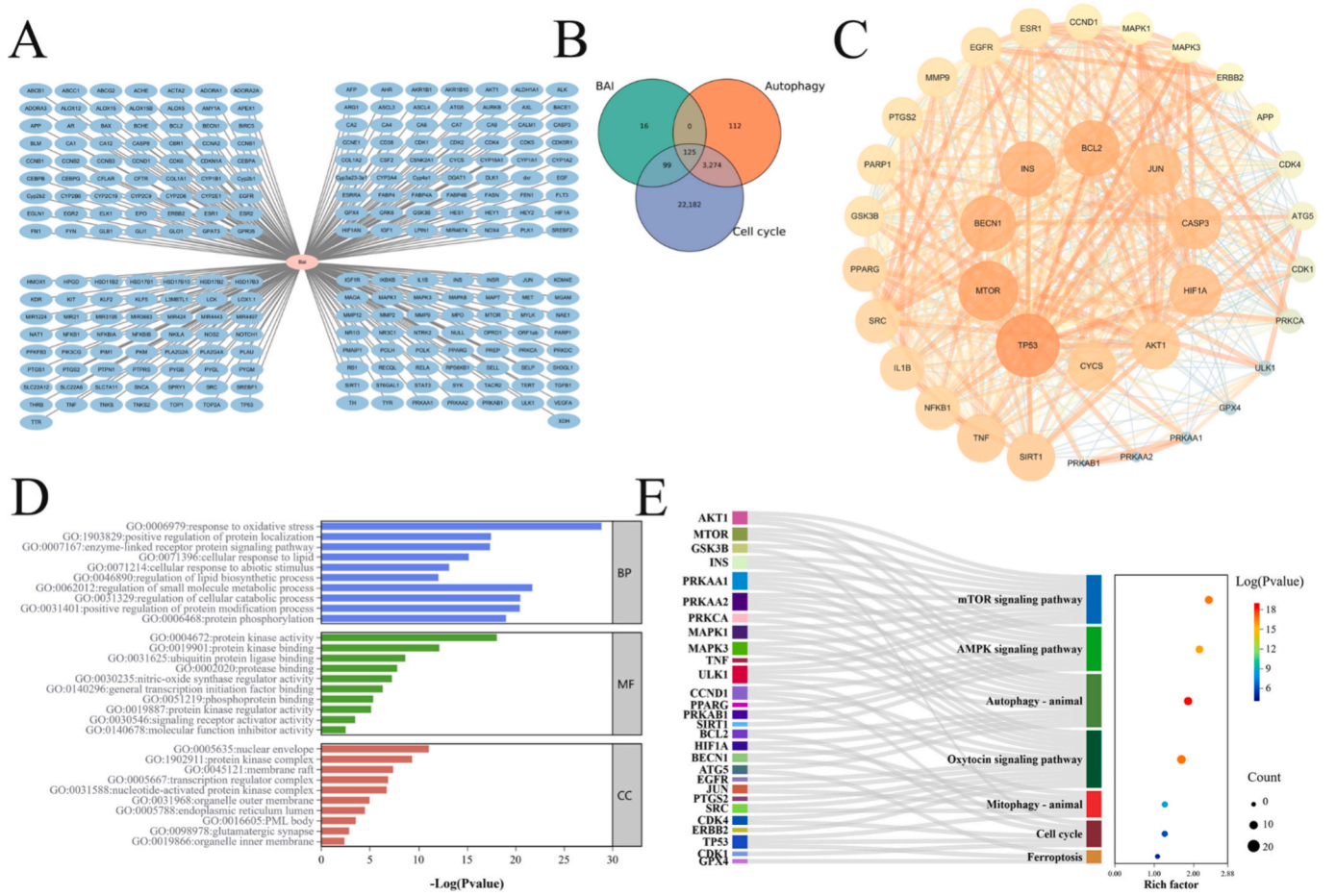

Fig. 7. Network pharmacology analysis of BAI and autophagy. (**A**) BAI target genes network. (**B**) Venn diagram. (**C**) PPI network diagram of key genes of BAI regulating autophagy and cell cycle. (**D**) GO enrichment analysis diagram. (**E**) KEGG pathway enrichment analysis diagram.

in this spacer region. Co-IP and confocal analysis verified that BAI interferes with the formation of the AMPK–ULK1 complex, molecular docking providing new insights for the analysis of drug effects. Yuan et al. confirmed that BAI significantly reduced p-AMPK/AMPK levels in a dose-dependent manner, protecting rats brains [45]. We found that the addition of BAI in vivo or in vitro inhibited CPF-induced AMPK pathway activation. Although Compound C can effectively inhibit AMPK, the effective dose may be toxic to cells [46]. BAI is a natural AMPK inhibitor with the advantages of low toxicity and few side effects. In summary, BAI mitigates CPF toxicity by binding to AMPK and preventing its interaction with ULK1.

The link between cell cycle and cell death patterns controls fundamental processes of growth and development throughout life [47]. Cell cycle arrest is closely related to the mode of cell death, with the S phase playing a crucial role [48]. AMPK activation induces cell cycle arrest in the S phase, and this arrest depends on p53 inhibition [49]. In this study, it was found that an AMPK activator effectively shifted the cell cycle from the G1 to S phase. RNA-seq results showed that CPF-induced intestinal toxicity was associated with cell cycle disruption. CPF exposure activated the AMPK pathway, suppressed the p53/p21 pathway, and caused cell cycle arrest in the S phase in carp midgut. Ventura et al. found that CPF exposure induced EPC cell cycle arrest in the S phase, consistent with the results of this study [50]. We have demonstrated that BAI can inhibit the cell cycle–blocking effects induced by CPF and the AMPK activator. Sulistyowati et al. showed that BAI can prevent cell cycle arrest and protect blood vessels in mice [51]. In addition, network pharmacological analysis reaffirmed that BAI regulates the cell cycle through its close link to the AMPK pathway.

Autophagy, described as a double-edged sword, can protect cells from injury and act as a cell death mechanism when activated by toxic substances [52,53]. The conversion of LC3B-I to LC3B-II is a crucial step in autophagy, and p62 serves as a substrate that is degraded during this process. ATG5 and ATG12 form a complex involved in autophagosome expansion [54]. As the core of autophagy, lysosomes provide the degradation capacity and play a crucial role in its regulation [18]. The AMPK–ULK1 complex enhances the recruitment of other key autophagy proteins, such as Beclin1 [55]. In addition, AMPK enhances the fusion of autophagosomes with lysosomes [56]. We found that the AMPK activator induces excessive autophagy, indicating that the AMPK–ULK1 pathway regulates this process. CPF induced autophagy in SH-SY5Y cells, accompanied by increased LC3-II and decreased p62 expression in a concentration-dependent manner [57]. In this study, CPF exposure caused lysosomal damage and abnormal expression of LC3B, p62, ATG5, and ATG12, indicating that CPF drives autophagy both in in vivo and in vitro models, which was further confirmed by experiments using the autophagy inhibitor CQ. Wu et al. reported that BAI suppressed autophagosome assembly in carp kidneys [20]. We confirmed that BAI counteracts the activation of autophagy by AMPK activators and CPF. Combined with the findings on the interaction between BAI and AMPK, this study indicates that BAI alleviates CPF-induced autophagy by inhibiting the AMPK–ULK1 pathway, thereby reducing tissue damage.

Ferroptosis is a recently discovered iron-dependent form of cell death. Several key pathways are involved, including disruptions in iron ion transport and lipid metabolism [15]. Lipid peroxides generated in cell cycle arrest contribute to the execution of ferroptosis [58]. Moreover, excessive autophagy may promote ferroptosis [19]. Iron is taken

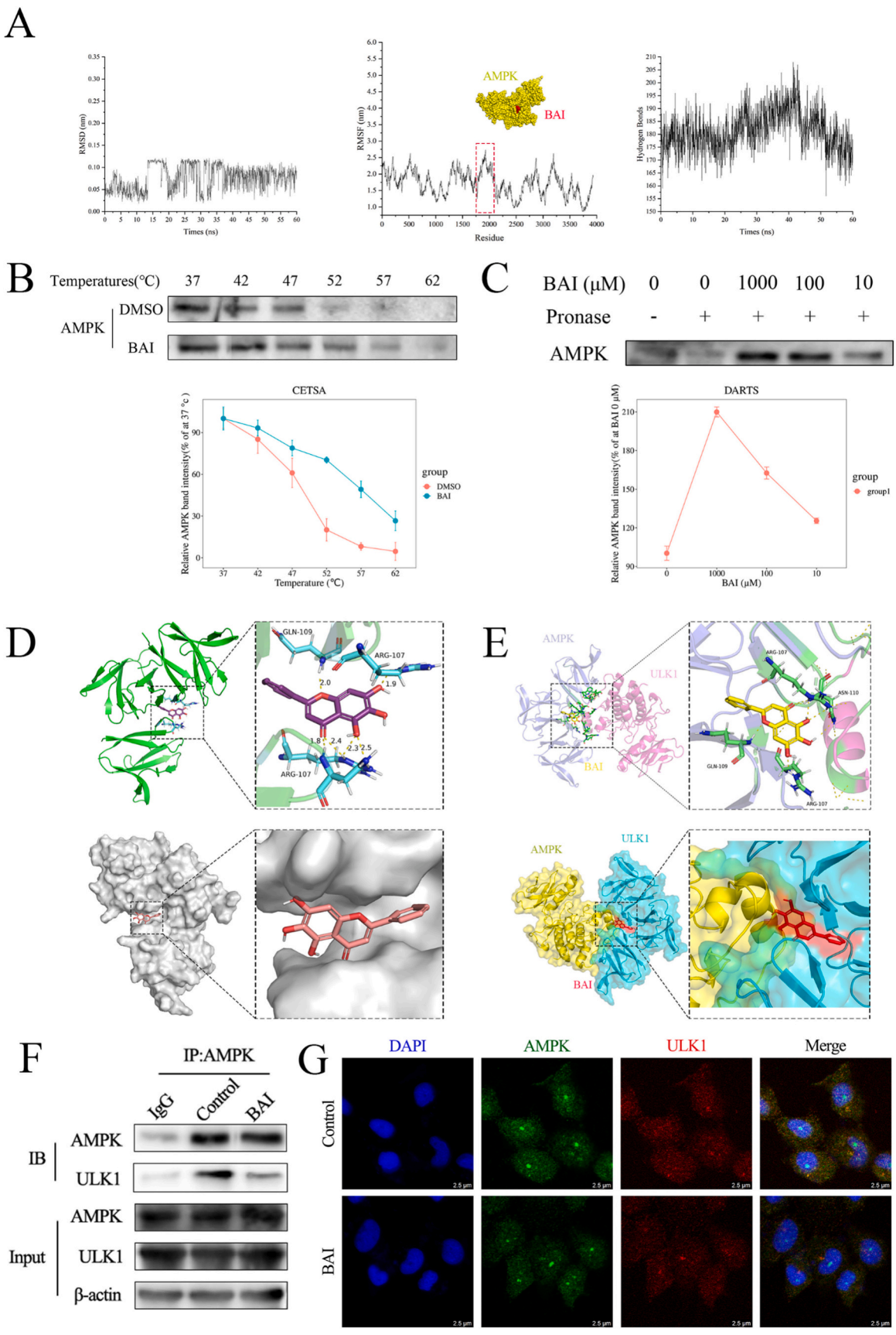

Fig. 8. BAI resists the effects of AMPK regulation on CPF-exposed carp intestine and EPC cells. (**A**) Molecular dynamics simulation results. (**B**) CETSA analysis results. (**C**) EPC cells were treated with DMSO or BAI and then exposed to MG132 (10 mM) for the specified time points. (**D-E**) Molecular docking of three-dimensional structure and protein structure. (**F**) WB of Co-IP results of AMPK and ULK1. (**G**) The representative images of immunofluorescence co-localization of AMPK and ULK1. All data were shown as mean ± SD (n = 3).

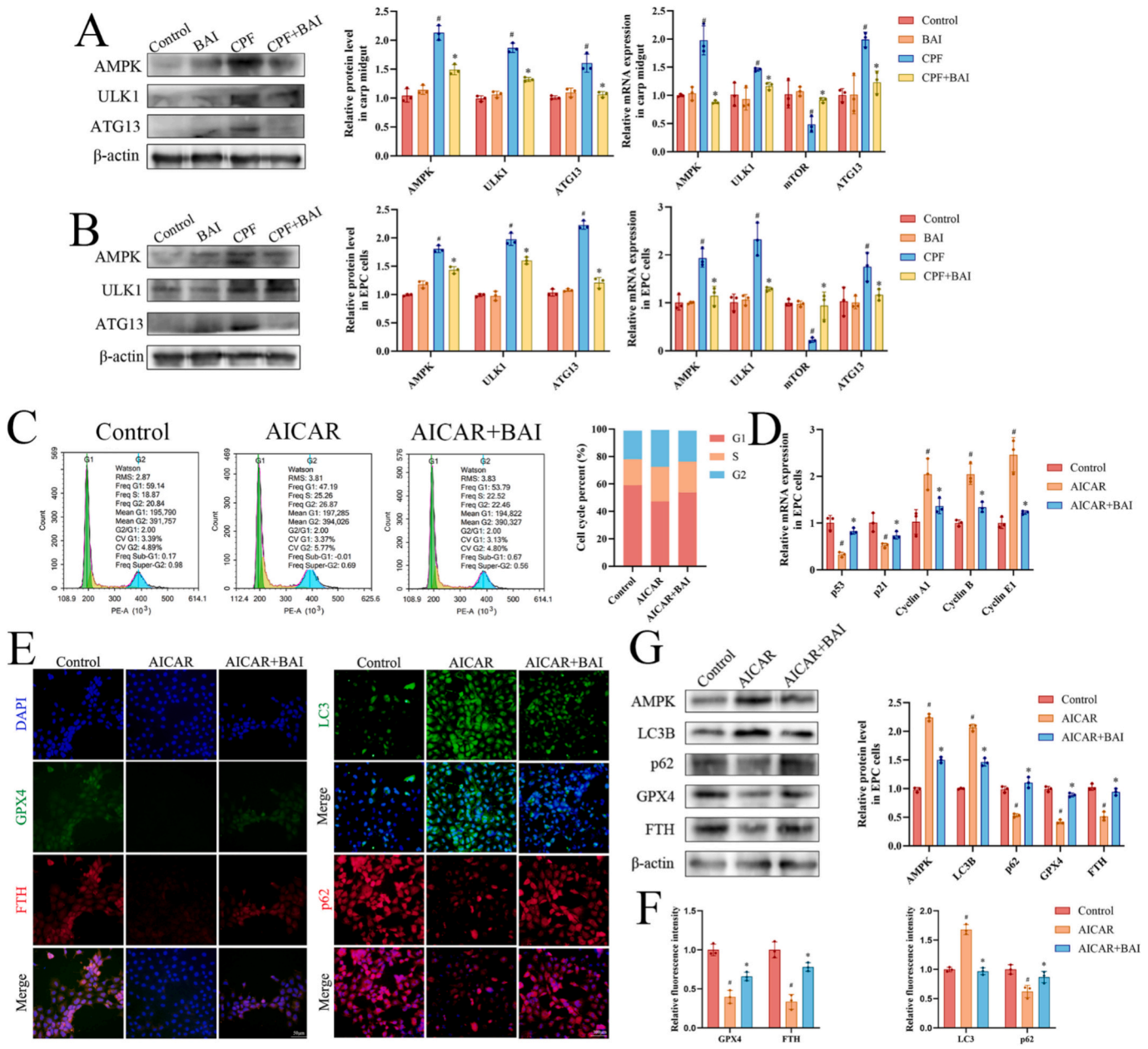

Fig. 9. Effects of AMPK activation on cell cycle, autophagy and ferroptosis. (**A-B**) Gene expression of AMPK pathway markers in carp midgut and EPC cells. (**C**) Results of cell cycle flow cytometry. (**D**) Cell cycle related mRNA expression levels. (**E-F**) Immunofluorescence double staining. (**G**) AMPK, LC3B, p62, GPX4 and FTH protein expression levels. $^{\#}$Represents the statistical difference between the group and the Control group. *Represents the statistical difference between the group and the CPF group. All data were shown as mean ± SD (n = 3). *P < 0.05, $^{\#}$P < 0.05.

up via transferrin and stored in ferritin, composed of ferritin heavy chain (FTH) and ferritin light chain [59,60]. Normally, iron is stored in lysosomes which helps maintain iron homeostasis. However, when lysosomes are damaged, large amounts of iron are released [61]. Simultaneously, FTH degradation releases Fe^{2+} and GPX4 inactivation leads to lipid metabolism disorders after autophagy initiation [62,63]. In this study, RNA-seq showed that the intestinal toxicity of CPF was mediated by ferroptosis, fatty acid metabolism, steroid biosynthesis, and fatty acid biosynthesis. We observed that CPF induced iron overload and GPX4 inactivation–mediated ferroptosis. Transcriptomics analysis revealed that ACSL4 is not activated by CPF, supporting the findings of Lee and Gan [64] who reported that ACSL4 is required for ferroptosis only in certain cases. He et al. reported that CQ can inhibit ferroptosis by blocking autophagic flux in mice liver [65]. Interestingly, we discovered that CQ inhibited ferroptosis, and that Fer-1 additionally affected autophagy after CPF exposure, demonstrating that autophagy and ferroptosis are mutually reinforcing. In addition, AMPK activation triggers iron overload. However, BAI effectively antagonized ferroptosis induced by both CPF and AMPK activators. Additionally, the specific amino acid binding sites and pharmacokinetic properties of BAI need to be further verified in various animal models to support its potential clinical application.

5. Conclusion

In summary, this study reveals a novel mechanism by which BAI alleviates the intestinal toxicity of CPF. BAI targets AMPK and disrupts its binding to ULK1, thereby inhibiting CPF-induced autophagy, ferroptosis, and cell cycle arrest. As a result, BAI mitigates damage to intestinal tissue and mitochondria. These findings highlight the functional

and mechanistic aspects of the protective effects of BAI against CPF in aquatic environments and may provide new insights into strategies for protecting aquatic animals from environmental pollution.

CRediT authorship contribution statement

Huanqi Zhang: Writing – original draft, Data curation, Conceptualization. **Xiaozhe Chen:** Validation, Software. **Fuqing Liu:** Visualization, Methodology. **Yanju Bi:** Investigation. **Meichen Gao:** Software. **Xiaojing Li:** Writing – review & editing, Supervision, Data curation, Conceptualization.

Author Agreement

We the undersigned declare that this manuscript entitled "Baicalein mitigates chlorpyrifos-induced intestinal injury by blocking AMPK-ULK1 binding via the autophagy/ferroptosis axis" is original, has not been published before and is not currently being considered for publication elsewhere.

We confirm that the manuscript has been read and approved by all named authors and that there are not other persons who satisfied the criteria for authorship but are not listed. We further confirm that the order of authors listed in the manuscript has been approved by all of us.

We understand that the corresponding author is the sole contact for the Editorial process. He is responsible for communicating with the other authors about progress, submissions of revisions and final approval of proofs.

Signed by all authors:

Author statement

All authors have read the manuscript and agreed to submit it in its current form for consideration for publication in the Journal

Declaration of competing interest

The authors declare that they have no known competing financial interests or personal relationships that could have appeared to influence the work reported in this paper.

Acknowledgement

This study is supported by the "Academic Backbone" Project and Student Innovation Practical Training Project of Northeast Agricultural University. The authors extend their sincere thanks to the members of the veterinary internal medicine laboratory and key Laboratory for Laboratory Animals at the College of Veterinary Medicine, Northeast Agricultural University. We thank the CNSknowall platform (https://cnsknowall.com/#/HomePage) for providing a plotting platform.Graphical abstract: created in BioRender. Zhang, H. (2025) https://BioRender.com/k28v011.

Appendix A. Supplementary data

Supplementary data to this article can be found online at https://doi.org/10.1016/j.intimp.2025.115382.

Data availability

Data will be made available on request.

References

[1] E.M. John, J.M. Shaike, Chlorpyrifos: pollution and remediation, Environ. Chem. Lett. 13 (2015) 269–291, https://doi.org/10.1007/s10311-015-0513-7.
[2] Y. Huang, W. Zhang, S. Pang, J. Chen, P. Bhatt, S. Mishra, et al., Insights into the microbial degradation and catalytic mechanisms of chlorpyrifos, Environ. Res. 194 (2021) 110660, https://doi.org/10.1016/j.envres.2020.110660.
[3] A. Raj, A. Kumar, Recent advances in assessment methods and mechanism of microbe-mediated chlorpyrifos remediation, Environ. Res. 214 (2022), https://doi.org/10.1016/j.envres.2022.114011.
[4] F.K. Sishu, S.A. Tilahun, P. Schmitter, G. Assefa, T.S. Steenhuis, Pesticide contamination of surface and groundwater in an Ethiopian highlands' watershed, WATER 14 (2022), https://doi.org/10.3390/w14213446.
[5] J.L.D.P. Lu, Multipesticide residue assessment of agricultural soil and water in major farming areas in Benguet, Philippines, Arch. Environ. Contam. Toxicol. 59 (2010) 175–181, https://doi.org/10.1007/s00244-010-9478-5.
[6] M. Hasanuzzaman, M.A. Rahman, M.S. Islam, M.A. Salam, M.R. Nabi, Pesticide residues analysis in water samples of Nagarpur and Saturia Upazila, Bangladesh, Appl Water Sci 8 (2018) 8, https://doi.org/10.1007/s13201-018-0655-4.
[7] J.A. Campillo, M. Albentosa, N.J. Valdés, R. Moreno-González, V.M. León, Impact assessment of agricultural inputs into a Mediterranean coastal lagoon (mar Menor, SE Spain) on transplanted clams (Ruditapes decussatus) by biochemical and physiological responses, Aquat. Toxicol. 142-143 (2013) 365–379, https://doi.org/10.1016/j.aquatox.2013.09.012.
[8] J. Reygner, C.J. Condette, A. Bruneau, S. Delanaud, L. Rhazi, F. Depeint, et al., Changes in composition and function of human intestinal microbiota exposed to Chlorpyrifos in oil as assessed by the SHIME® model, Int. J. Environ. Res. Public Health 13 (2016), https://doi.org/10.3390/ijerph13111088.
[9] N. Xu, Z. Zhou, B. Chen, Z. Zhang, J. Zhang, Y. Li, et al., Effect of chlorpyrifos on freshwater microbial community and metabolic capacity of zebrafish, Ecotoxicol. Environ. Saf. 262 (2023) 115230, https://doi.org/10.1016/j.ecoenv.2023.115230.
[10] H. Fu, H. Liu, Y. Ge, Y. Chen, P. Tan, J. Bai, et al., Chitosan oligosaccharide alleviates and removes the toxicological effects of organophosphorus pesticide chlorpyrifos residues, J. Hazard. Mater. 446 (2023), https://doi.org/10.1016/j.jhazmat.2022.130669.
[11] P. Li, X. Ma, D. Liu, Y. Wei, P. Li, H. Hou, et al., A microbiome abundant environment remodels the intestinal microbiota and improves resistance to obesity induced by chlorpyrifos in mice*, Environ. Pollut. 315 (2022), https://doi.org/10.1016/j.envpol.2022.120415.
[12] Y. Yang, S. Ma, Z. Yan, F. Liu, Q. Diao, P. Dai, Effects of three common pesticides on survival, food consumption and midgut bacterial communities of adult workers Apis cerana and Apis mellifera, Environ. Pollut. 249 (2019) 860–867, https://doi.org/10.1016/j.envpol.2019.03.077.
[13] T.-L. Ma, J.-X. Chen, P. Zhu, C.-B. Zhang, Y. Zhou, J.-X. Duan, Focus on ferroptosis regulation: exploring novel mechanisms and applications of ferroptosis regulator, Life Sci. 307 (2022), https://doi.org/10.1016/j.lfs.2022.120868.
[14] T. Yao, L. Li, The influence of microbiota on ferroptosis in intestinal diseases, Gut Microbes 15 (2023), https://doi.org/10.1080/19490976.2023.2263210.
[15] T. Xu, J. Cui, R. Xu, J. Cao, M.-y. Guo, Microplastics induced inflammation and apoptosis via ferroptosis and the NF-κB pathway in carp, Aquat. Toxicol. 262 (2023) 106659, https://doi.org/10.1016/j.aquatox.2023.106659.
[16] P. Sen Gupta, S. Karmakar, I. Biswas, J. Ghosal, A. Banerjee, S. Roy, et al., Vitamin E alleviates chlorpyrifos induced glutathione depletion, lipid peroxidation and iron accumulation to inhibit ferroptosis in hepatocytes and mitigate toxicity in zebrafish, Chemosphere 359 (2024) 142252, https://doi.org/10.1016/j.chemosphere.2024.142252.
[17] J. Liu, G. Yang, H. Zhang, Glyphosate-triggered hepatocyte ferroptosis via suppressing Nrf2/GSH/GPX4 axis exacerbates hepatotoxicity, Sci. Total Environ. 862 (2023) 160839, https://doi.org/10.1016/j.scitotenv.2022.160839.
[18] W.W.-Y. Yim, N. Mizushima, Lysosome biology in autophagy, Cell discovery 6 (2020) 6, https://doi.org/10.1038/s41421-020-0141-7.
[19] Y. Xie, Y. Zhou, J. Wang, L. Du, Y. Ren, F. Liu, Ferroptosis, autophagy, tumor and immunity, HELIYON 9 (2023), https://doi.org/10.1016/j.heliyon.2023.e19799.
[20] Q. Wu, W. Yang, Y. Bi, Y. Yao, C. Li, X. Li, Baicalein inhibits apoptosis and autophagy induced by chlorpyrifos exposure to kidney of Cyprinus carpio through activation of PI3K/AKT pathway, Pestic. Biochem. Physiol. 196 (2023) 105624, https://doi.org/10.1016/j.pestbp.2023.105624.
[21] S. Herzig, R.J. Shaw, AMPK: guardian of metabolism and mitochondrial homeostasis, Nat. Rev. Mol. Cell Biol. 19 (2018) 121–135, https://doi.org/10.1038/nrm.2017.95.
[22] E.G. Foerster, T. Mukherjee, L. Cabral-Fernandes, J.D.B. Rocha, S.E. Girardin, D. J. Philpott, How autophagy controls the intestinal epithelial barrier, Autophagy 18 (2022) 86–103, https://doi.org/10.1080/15548627.2021.1909406.
[23] Z. Miao, Z. Miao, S. Feng, S. Xu, Chlorpyrifos-mediated mitochondrial calcium overload induces EPC cell apoptosis via ROS/AMPK/ULK1, Fish Shellfish Immunol. 141 (2023) 109053, https://doi.org/10.1016/j.fsi.2023.109053.
[24] X. Sun, W. Zhang, Y. Wang, Y. Zhang, X. Liu, X. Shi, et al., Combined exposure to di (2-ethylhexyl) phthalate and polystyrene microplastics induced renal autophagy through the ROS/AMPK/ULK1 pathway, Food Chem. Toxicol. 171 (2023) 113521, https://doi.org/10.1016/j.fct.2022.113521.
[25] W. Sun, Y. Lei, Z. Jiang, K. Wang, H. Liu, T. Xu, BPA and low-Se exacerbate apoptosis and mitophagy in chicken pancreatic cells by regulating the PTEN/PI3K/AKT/mTOR pathway, J. Adv. Res. (2024), https://doi.org/10.1016/j.jare.2024.01.029.
[26] Y. Du, Y. Han, R. Zhang, Y. Zhang, S. Bao, Y. Cao, Dietary baicalein improves growth performance, antioxidant activity, and intestinal flora of koi carp (Cyprinus carpio), Aquaculture Rep. 27 (2022), https://doi.org/10.1016/j.aqrep.2022.101421.
[27] X. Li, Q. Wu, D. Chen, Y. Bai, Y. Yang, S. Xu, Environment-relevant concentrations of cadmium induces necroptosis and inflammation; baicalein maintains gill

homeostasis through suppressing ROS/ER stress signaling in common carps (Cyprinus carpio L.), Environ. Pollut. 340 (2024), https://doi.org/10.1016/j.envpol.2023.122805.
[28] B. Zhang, Y. Dong, N. Yu, Y. Sun, Y. Xing, F. Yang, et al., Intestinal metabolism of baicalein after oral administration in mice: pharmacokinetics and mechanisms, J. Funct. Foods 54 (2019) 53–63, https://doi.org/10.1016/j.jff.2018.12.037.
[29] S. Guo, L. Zhou, X. Liu, L. Gao, Y. Li, Y. Wu, Baicalein alleviates cisplatin-induced acute kidney injury by inhibiting ALOX12-dependent ferroptosis, PHYTOMEDICINE 130 (2024), https://doi.org/10.1016/j.phymed.2024.155757.
[30] M. Yu, H. Li, B. Wang, Z. Wu, S. Wu, G. Jiang, et al., Baicalein ameliorates polymyxin B-induced acute renal injury by inhibiting ferroptosis via regulation of SIRT1/p53 acetylation, Chem. Biol. Interact. 382 (2023), https://doi.org/10.1016/j.cbi.2023.110607.
[31] D. Goś, "Be healthy as a fish" educational program – presenting how zebrafish can improve our understanding of human diseases, Dev. Biol. 457 (2020) 169–171, https://doi.org/10.1016/j.ydbio.2019.01.012.
[32] J. Liu, W. Zhang, X. Li, S. Xu, New insights into Baicalein's effect on Chlorpyrifos-induced liver injury in carp: involving macrophage polarization and Pyropto sis, J. Agric. Food Chem. (2023), https://doi.org/10.1021/acs.jafc.2c08580.
[33] Y. Bi, H. Wei, Y. Chai, H. Wang, Q. Xue, J. Li, Intermittent mild cold acclimation ameliorates intestinal inflammation and immune dysfunction in acute cold-stressed broilers by regulating the TLR4/MyD88/NF-kappaB pathway, Poult. Sci. 103 (2024) 103637, https://doi.org/10.1016/j.psj.2024.103637.
[34] H. Xing, C. Wang, H. Wu, D. Chen, S. Li, S. Xu, Effects of atrazine and chlorpyrifos on DNA methylation in the brain and gonad of the common carp, Comp. Biochem. Physiol. C. Toxicol. Pharmacol. 168 (2015) 11–19, https://doi.org/10.1016/j.cbpc.2014.11.002.
[35] X. Xie, W. Lin, W. Zheng, T. Chen, H. Yang, L. Sun, et al., Downregulation of G2/mitotic-specific cyclinB1 triggers autophagy via AMPK-ULK1-dependent signal pathway in nasopharyngeal carcinoma cells, Cell Death Dis. 10 (2019), https://doi.org/10.1038/s41419-019-1369-8.
[36] N.K. Nandi, A. Vyas, M.J. Akhtar, B. Kumar, The growing concern of chlorpyrifos exposures on human and environmental health, Pestic. Biochem. Physiol. 185 (2022) 105138, https://doi.org/10.1016/j.pestbp.2022.105138.
[37] X. Wang, X. Tan, J. Zhang, J. Wu, H. Shi, The emerging roles of MAPK-AMPK in ferroptosis regulatory network, Cell Commun. Signal. 21 (2023), https://doi.org/10.1186/s12964-023-01170-9.
[38] J. Rodencal, N. Kim, V.L. Li, A. He, M. Lange, J. He, et al., A cell cycle-dependent ferroptosis sensitivity switch governed by EMP2, bioRxiv : The Preprint Server for Biol. (2023), https://doi.org/10.1101/2023.07.19.549715.
[39] Z. Li, X. Tian, X. Ji, J. Wang, H. Chen, D. Wang, et al., ULK1-ATG13 and their mitotic phospho-regulation by CDK1 connect autophagy to cell cycle, PLoS Biol. 18 (2020), https://doi.org/10.1371/journal.pbio.3000288.
[40] D.L. Schmitt, Imaging subcellular AMPK activity using an excitation-Ratiometric AMPK activity reporter, Current protocols 3 (2023) e771, https://doi.org/10.1002/cpz1.771.
[41] J. Kim, M. Kundu, B. Viollet, K.-L. Guan, AMPK and mTOR regulate autophagy through direct phosphorylation of Ulk1, Nat. Cell Biol. 13 (2011) 132–U171, https://doi.org/10.1038/ncb2152.
[42] J.-M. Park, D.-H. Lee, D.-H. Kim, Redefining the role of AMPK in autophagy and the energy stress response, Nat. Commun. 14 (2023) 2994, https://doi.org/10.1038/s41467-023-38401-z.
[43] M. Bach, M. Larance, D.E. James, G. Ramm, The serine/threonine kinase ULK1 is a target of multiple phosphorylation events, Biochem. J. 440 (2011) 283–291, https://doi.org/10.1042/bj20101894.
[44] H.I.D. Mack, B. Zheng, J.M. Asara, S.M. Thomas, AMPK-dependent phosphorylation of ULK1 regulates ATG9 localization, AUTOPHAGY 8 (2012) 1197–1214, https://doi.org/10.4161/auto.20586.
[45] Y. Yuan, W. Men, X. Shan, H. Zhai, X. Qiao, L. Geng, et al., Baicalein exerts neuroprotective effect against ischaemic/reperfusion injury via alteration of NF-kB and LOX and AMPK/Nrf2 pathway, INFLAMMOPHARMACOLOGY 28 (2020) 1327–1341, https://doi.org/10.1007/s10787-020-00714-6.
[46] Y.-C. Lee, J.-T. Chiou, L.-S. Chang, AMPK inhibition induces MCL1 mRNA destabilization via the p38 MAPK/ miR-22/HuR axis in chronic myeloid leukemia cells, Biochem. Pharmacol. 209 (2023), https://doi.org/10.1016/j.bcp.2023.115442.
[47] L.V. Loftus, S.R. Amend, K.J. Pienta, Interplay between cell death and cell proliferation reveals new strategies for Cancer therapy, Int. J. Mol. Sci. 23 (2022), https://doi.org/10.3390/ijms23094723.
[48] S. Tone, S. Tanaka, Analysis of relationship between programmed cell death and cell cycle in limb-bud, Horm. Res. 48 (1997) 5–10, https://doi.org/10.1159/000191293.
[49] R.G. Jones, D.R. Plas, S. Kubek, M. Buzzai, J. Mu, Y. Xu, et al., AMP-activated protein kinase induces a p53-dependent metabolic checkpoint, Mol. Cell 18 (2005) 283–293, https://doi.org/10.1016/j.molcel.2005.03.027.
[50] C. Ventura, M. Nunez, N. Miret, D.M. Lamas, A. Randi, A. Venturino, et al., Differential mechanisms of action are involved in chlorpyrifos effects in estrogen-dependent or -independent breast cancer cells exposed to low or high concentrations of the pesticide, Toxicol. Lett. 213 (2012) 184–193, https://doi.org/10.1016/j.toxlet.2012.06.017.
[51] E. Sulistyowati, S.-E. Huang, T.-L. Cheng, Y.-Y. Chao, C.-Y. Li, C.-W. Chang, et al., Vasculoprotective potential of Baicalein in angiotensin II-infused abdominal aortic aneurysms through inhibiting inflammation and oxidative stress, Int. J. Mol. Sci. 24 (2023), https://doi.org/10.3390/ijms242116004.
[52] S. Orrenius, V.O. Kaminskyy, B. Zhivotovsky, in: P.A. Insel (Ed.), Autophagy in Toxicology: Cause or Consequence? 53, ANNUAL REVIEW OF PHARMACOLOGY AND TOXICOLOGY, 2013, pp. 275–297.
[53] Y. Shi, H.-M. Shen, V. Gopalakrishnan, N. Gordon, Epigenetic regulation of autophagy beyond the cytoplasm: a review, Front. Cell Dev. Biol. (2021), https://doi.org/10.3389/fcell.2021.675599.
[54] H. Changotra, S. Kaur, S.S. Yadav, G.L. Gupta, J. Parkash, A. Duseja, ATG5: a central autophagy regulator implicated in various human diseases, Cell Biochem. Funct. 40 (2022) 650–667, https://doi.org/10.1002/cbf.3740.
[55] R. Saikia, J. Joseph, AMPK: a key regulator of energy stress and calcium-induced autophagy, J. Mol. Med. 99 (2021) 1539–1551, https://doi.org/10.1007/s00109-021-02125-8.
[56] S. Wang, H. Li, M. Yuan, H. Fan, Z. Cai, Role of AMPK in autophagy, Front. Physiol. 13 (2022), https://doi.org/10.3389/fphys.2022.1015500.
[57] J.H. Park, J.E. Lee, I.C. Shin, H.C. Koh, Autophagy regulates chlorpyrifos-induced apoptosis in SH-SY5Y cells, Toxicol. Appl. Pharmacol. 268 (2013) 55–67, https://doi.org/10.1016/j.taap.2013.01.013.
[58] T. Homma, S. Kobayashi, J. Fujii, Methionine deprivation reveals the pivotal roles of cell cycle progression in Ferroptosis that is induced by cysteine starvation, CELLS 11 (2022), https://doi.org/10.3390/cells11101603.
[59] Y. Xiao, Z. Xu, Y. Cheng, R. Huang, Y. Xie, H.-I. Tsai, et al., Fe3+-binding transferrin nanovesicles encapsulating sorafenib induce ferroptosis in hepatocellular carcinoma, Biomater. Res. 27 (2023), https://doi.org/10.1186/s40824-023-00401-x.
[60] E.C. Theil, Ferritin: structure, gene regulation, and cellular function in animals, plants, and microorganisms, Annu. Rev. Biochem. 56 (1987) 289–315, https://doi.org/10.1146/annurev.bi.56.070187.001445.
[61] Y. Feng, H. Wei, M. Lyu, Z. Yu, J. Chen, X. Lyu, et al., Iron retardation in lysosomes protects senescent cells from ferroptosis, Aging 16 (2024) 7683–7703, https://doi.org/10.18632/aging.205777.
[62] D.C. Fuhrmann, A. Mondorf, J. Beifuss, M. Jung, B. Bruene, Hypoxia inhibits ferritinophagy, increases mitochondrial ferritin, and protects from ferroptosis, Redox Biol. 36 (2020), https://doi.org/10.1016/j.redox.2020.101670.
[63] W.S. Yang, K.J. Kim, M.M. Gaschler, M. Patel, M.S. Shchepinov, B.R. Stockwell, Peroxidation of polyunsaturated fatty acids by lipoxygenases drives ferroptosis, Proc. Natl. Acad. Sci. USA 113 (2016) E4966–E4975, https://doi.org/10.1073/pnas.1603244113.
[64] H. Lee, B. Gan, Ferroptosis execution: is it all about ACSL4? Cell Chem. Biol. 29 (2022) 1363–1365, https://doi.org/10.1016/j.chembiol.2022.08.002.
[65] Z. He, P. Shen, L. Feng, H. Hao, Y. He, G. Fan, et al., Cadmium induces liver dysfunction and ferroptosis through the endoplasmic stress-ferritinophagy axis, Ecotoxicol. Environ. Saf. 245 (2022), https://doi.org/10.1016/j.ecoenv.2022.114123.